Laser Photonics Rev. 7, No. 5, L45–L50 (2013) / DOI 10.1002/lpor.201300035

LASER & PHOTONICS REVIEWS

Abstract Compact semiconductor light sources with high performance continuous-wave (CW) and single mode operation are highly demanded for many applications in the terahertz (THz) frequency range. Distributed feedback (DFB) and photonic crystal (PhC) quantum cascade (QC) lasers are amongst the leading candidates in this field. Absorbing boundary condition is a commonly used method to control the optical performance of a laser in double-metal confinement. However, this approach increases the total loss in the device and results in a large threshold current density, limiting the CW maximum output power and operating temperature. In this letter, a robust surface emitting continuous-wave terahertz QC laser is realized in a two-dimensional PhC structure by a second order Bragg grating extractor that simultaneously provides the boundary condition necessary for mode selection. This results in a 3.12 THz single mode CW operation with a 3 mW output power and a maximum operation temperature (T_{max}) of 100 K. Also, a highly collimated far-field pattern is demonstrated, which is an important step towards real world applications.

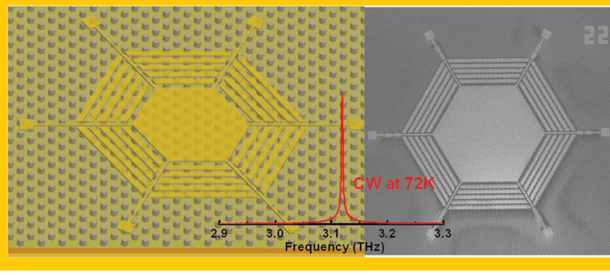

LETTER ARTICLE

Continuous-wave vertically emitting photonic crystal terahertz laser

Zhaolu Diao[1,], Christopher Bonzon[2,**], Giacomo Scalari[2], Mattias Beck[2], Jérôme Faist[2], and Romuald Houdré[1,*]**

1. Introduction

Since the first quantum cascade (QC) laser was demonstrated in 1994 [1] and implemented in THz regime (0.1-10 THz) in 2002 [2], they have become one of the most important solid state light sources in this frequency range. The metal-metal (MM) waveguide was a key improvement in applying the quantum cascade concept from mid-infrared to THz range, MM waveguides are inherently broadband and allow for a sub-wavelength field confinement, ratio of down to $\lambda/50$ [3–5]. Nevertheless, this confinement leads to a highly divergent beam from the facet. Different strategies like photonic crystal (PhC) or metallic grating DFB [6] patterning for in plane or vertical emission have already been demonstrated. Monochromatic, low divergence, vertical emission THz lasers with low threshold current density (J_{th}) and high maximum operation temperature (T_{max}) have been achieved [7–12]. However, most of these progresses were demonstrated in pulsed operation mode. Continuous-wave (CW) operation performance is still limited and far from being optimized, despite the fact that it is of a crucial demand in astrophysics, biology, sensing, environmental and pollutant monitoring, or security screening [13–16].

For the best of the QC laser and PhC QC laser reported so far in the THz range, T_{max} of CW operation are 117 K [17] and 85 K [10] respectively [10, 18, 19]. Because of the optimum overlap between the optical mode and the gain region and the possibility to fabricate very high Q and compact cavities, high index contrast photonic crystals have a very good potential for high performance CW operation compared to competing approaches[10, 20]. Both the PhC QC laser and metallic grating DFB laser rely on an absorbing or reflecting boundary condition for laser mode-control and for achieving better far-field patterns [21]. In the previous demonstrations, the energy dissipated at the boundaries does not contribute to the lasing emission, which additionally challenges the CW performance of the lasing device.

In previous reports, PhC 1st band edge in-plane emission and PhC 3rd band edge vertical emission QC lasers have demonstrated the advantages of PhC approaches in term of single mode operation, reduction of losses and better pumping efficiency [11, 12]. Compared to other PhC QC lasers, which only have PhC structures in the top metal layer, similar methods also used in this work bring three main advantages. Firstly, the in-plane propagation of an electromagnetic wave experiences a two-dimensional (2D) PhC modulation provided by the high index mismatch (refractive index contrast 1.90: 3.45). This modulation results in an effective PhC gain enhancement of the band edge mode and improves the monochromic operation of the device. Secondly, the mode at the first band edge K point is a dielectric band edge mode. The major fraction

[1] Ecole Polytechnique Fédérale de Lausanne (EPFL), Institut de Physique de la Matière Condensée, Lausanne, CH-1015, Switzerland
[2] Eidgenössische Technische Hochschule Zürich (ETHZ), Institut für Quantenelektronik, Zürich, CH-8072, Switzerland
[**] These authors contributed equally to this work.
[*] Corresponding author: e-mail: romuald.houdre@epfl.ch

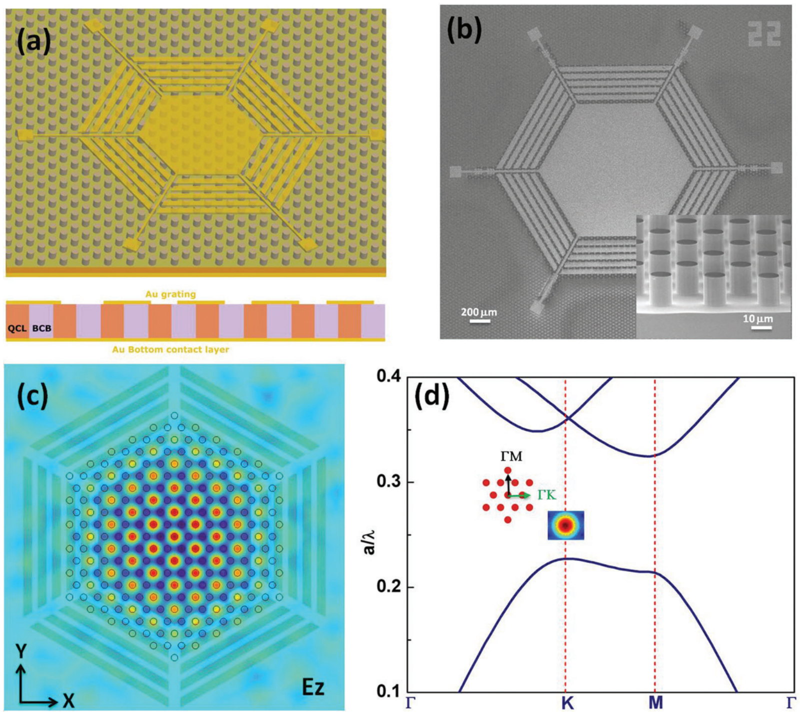

Figure 1 Device details and design. (a) 3D schematic view of the device and side view of Bragg extractor part. (b) Scanning electron micrograph of a typical device (top pumping pas diameter 1000 μm, period of the grating Λ 47 μm, duty cycle 62%, lattice constant **a** 22 μm, filling factor 30%), inset: PhC QC pillars after ICP dry etching and before BCB planarization. (c) Out-of-plane electric field ($\mathbf{E_z}$) distribution of the device with 3D finite element methods (COMSOL). (d) Transverse magnetic photonic band structure of the triangular lattice used in the design (filling factor is 30%).

of the electric field is distributed inside the high dielectric constant media consisting of QC pillars. A lower area of QC active material is pumped (filling factor filling factor of 20% or 30%) which results in an improvement of the electrical pumping efficiency. Thirdly, by filling the empty volume between QC pillars with low loss (3 cm^{-1} at 3.1 THz and 300 K) Benzocyclobutene (BCB), the surface to volume ratio and heat flow inside the device are improved by diluting the active region without significantly increasing the total loss [22]. In the present work, the loss type boundary conditions which have been used in PhC and DFB QC laser [8, 23] is replaced by a second order Bragg grating. This grating has multiple-functions. As a second order Bragg grating, it can diffract TM polarized in-plane radiation at the required frequency into vertical emission. More importantly, instead of absorbing the radiation at the boundary, to ensure the single mode operation this Bragg grating scatters them into desired vertical emission. As a consequence, this design shows significant improvement for CW operation in terms of maximum output power and T_{max}.

2. Design of the lasers

The QC laser used in this work has a $GaAs/Al_{0.15}Ga_{0.85}As$ heterostructure active layer with a hybrid of resonant phonon and bound to continuum scheme [24]. This 11 μm thick active layer operates at 3.1 THz with a gain band width of 0.6 THz. 2D triangular PhC patterns are defined in the QC active layer by inductively coupled plasma (ICP) dry etching (Fig. 1). The first PhC band edge K point mode frequency is chosen by appropriately selecting the lattice constant ***a*** and filling factor. Ultra smooth surface (less than 0.3% roughness) and a nearly perfect vertical side wall (vertical angle 89.9°) of the QC pillars can be observed in the inset scanning electron microscope (SEM) image of Fig. 1b. This is a critical factor in reducing the scattering and absorption losses due to the structural imperfections inside the device as much as possible.

The vertical field confinement of the QC laser is achieved by a 1 μm thick bottom Au layer by means of thermo-compressive gold-gold wafer bonding and a 1 μm thick top contact Au layer deposited with electron beam evaporation and lift-off. The hexagonal central pad corresponds to the hexagonal symmetry of the triangular lattice. The simulated electric field of the lasing mode has a centro-symmetric distribution at the edge of the central pumping pad with respect to the central pillar (Fig. 1c). Such in-phase radiation results in a constructive beam pattern in the far field. The device is electrically pumped via six centro-symmetric bonding pads (70 × 70 μm^2) which are 300 μm away from the central pumping pad. A series of metallic absorbers (maximum absorbing frequency at 3.1 THz) are inserted in between the central pumping pad and the bonding pads to prevent feedback and uncontrolled THz emission from the six bonding pads. A new type of vertical emission extractor is designed so as to decrease the extra losses due to the absorbing boundary condition used in PhC QC lasers or DFB QC lasers. A second order Bragg Au grating is implemented in the ΓK direction (Fig. 1d) to select the radiation in this direction from any other directions (mainly in the ΓM). The parameters of this Bragg grating are defined by the Bragg condition: $m\lambda_B = 2n_{eff}\Lambda$ (λ_B is the Bragg wavelength, n_{eff} is the effective refractive index

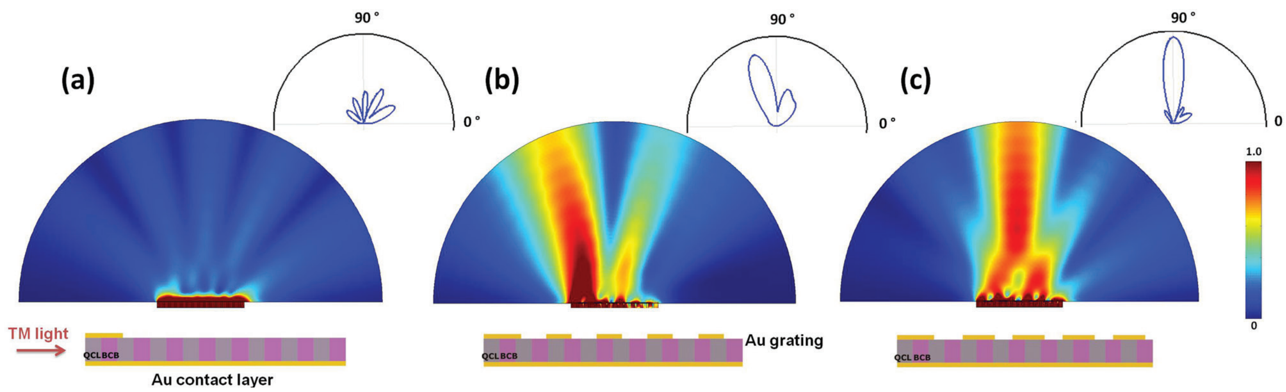

Figure 2 Effect of the Bragg extractor. (a) Simulated distribution of the electric field norm of the device without Bragg extractor. (b) and (c) Simulated distribution of the electric field norm of the device with standard (duty cycle 50%) and optimized Bragg extractors (duty cycle 62%) respectively. For each figure, inset is the polar plot of the electric field norm (the amplitude in inset of Fig. 2a has been multiplied by a factor of 2).

of the QC active layer, Λ is the period of the grating, m = 1, 2 . . .). Design of the 2nd order Bragg extractor was performed with the finite elements method (FEM). The 2D far field pattern of the devices with different configurations are compared (Fig. 2a–c: without extractor, with the standard Bragg extractor of 50% duty cycle and the optimized Bragg extractor of 62% duty cycle respectively) [25]. It can be seen that without the extractor, the limited part of the in-plane radiation which comes from the central pad is scattered out-of-plane with a divergent beam pattern. Improvements can be observed with the standard 2nd order Bragg extractor, the scattered radiation has two parts which are 10 degrees away from the vertical direction. After optimization of Λ, duty cycle and distance from the central pumping pad to the extractor, a considerable part of the in-plane radiation is scattered into vertical emission. A high intensity central beam pattern with a divergence angle less than 10 degrees is modeled with the optimized Bragg extractor.

3. Results and discussions

CW light-current-voltage (LIV) curves measured at different temperatures (50% duty cycle with long pulses and broad-area absolute power meter) for a single laser (the diameter of the central pumping pad is 600 μm, filling factor is 30%) are plotted in Fig. 3a. This device operates from 10 K up to 100 K with the maximum output power of 3 mW at 10 K. The LIV curve at 10 K shows a slope efficiency of 30 mW/A, meanwhile, the device has 1.2 mW output powers at 80 K (liquid nitrogen temperature is 77 K). In Fig. 3c, the CW spectrum measured at 72 K shows a single mode operation at 3.2 THz with a 25 dB side mode suppression ratio (not the maximum temperature for single mode operation). Compact and portable surface emission THz light source with mW level output power can be achieved under the help of a Stirling cryocooler (capable of cooling device down to 50 K or 40 K with 5 W or 15 W power dissipation [26]). The pulsed single mode operation of this laser shows a J_{th} of 300 Acm^{-2} at 10 K and T_{max} of 120 K. The limited differences in laser performance between the pulsed and CW operation prove the high pumping efficiency and effective heat transfer scheme of this design. CW LIV curves at different temperatures and spectrum at 10 K for another laser with different filling factor (the diameter of the central pumping pad is 600 μm, filling factor is 20%) are plotted in Fig. 3b and 3d. This device operates up to 90 K with the maximum output power of 6.5 mW at 10 K. For the same filling factor, devices (filling factor 30%) with different lattice constants (19, 20, 21 and 22 μm) show a photolithographic tuning range from 2.95 to 3.45 THz (Fig. 3e). The output power and T_{max} also show a dependence on the size of the device. As expected, the maximum output power increases with the dimension of the device. A larger device (the diameter of the central pumping pad is 1000 μm, filling factor is 30%) has a lower J_{th} (275 Acm^{-2}), slope efficiency (20 mW/A) and T_{max} (89 K) than those of a smaller device (for 600 μm device with filling factor 30%, J_{th}, slope efficiency and T_{max} are 295 Acm^{-2}, 30 mW/A and 100 K). The reasons for these differences are due to the smaller losses and lower heat flow efficiency inside of the larger device than those of the smaller one. The CW operation improvements of this design are summarized in Fig. 3f. The experimental results of the similar sized (the diameter of the central pumping pad is 600 μm) devices with different filling factor (20%, 30% and 40%) are compared with the case of in-plane emission FP device (1000*150 μm^2). The above mentioned devices are processed with the same QC layer. By decreasing the filling factor from 40% to 20%, the slope efficiency increases from 18 to 100 mW/A as a result of the higher electrically pumping efficiency. T_{max} increases as a result of the better heat flow and improved surface to volume ratio in the device. T_{max} of 30% device (100 K) is 42 K higher than that of FP laser (58 K). The increase in the total loss induced by decreasing the overlap between the band edge mode and the QC pillar (67.5% and 48.0% for filling factor 40% and 20%, respectively) explains the decrease of T_{max} from 100 K of 30% device

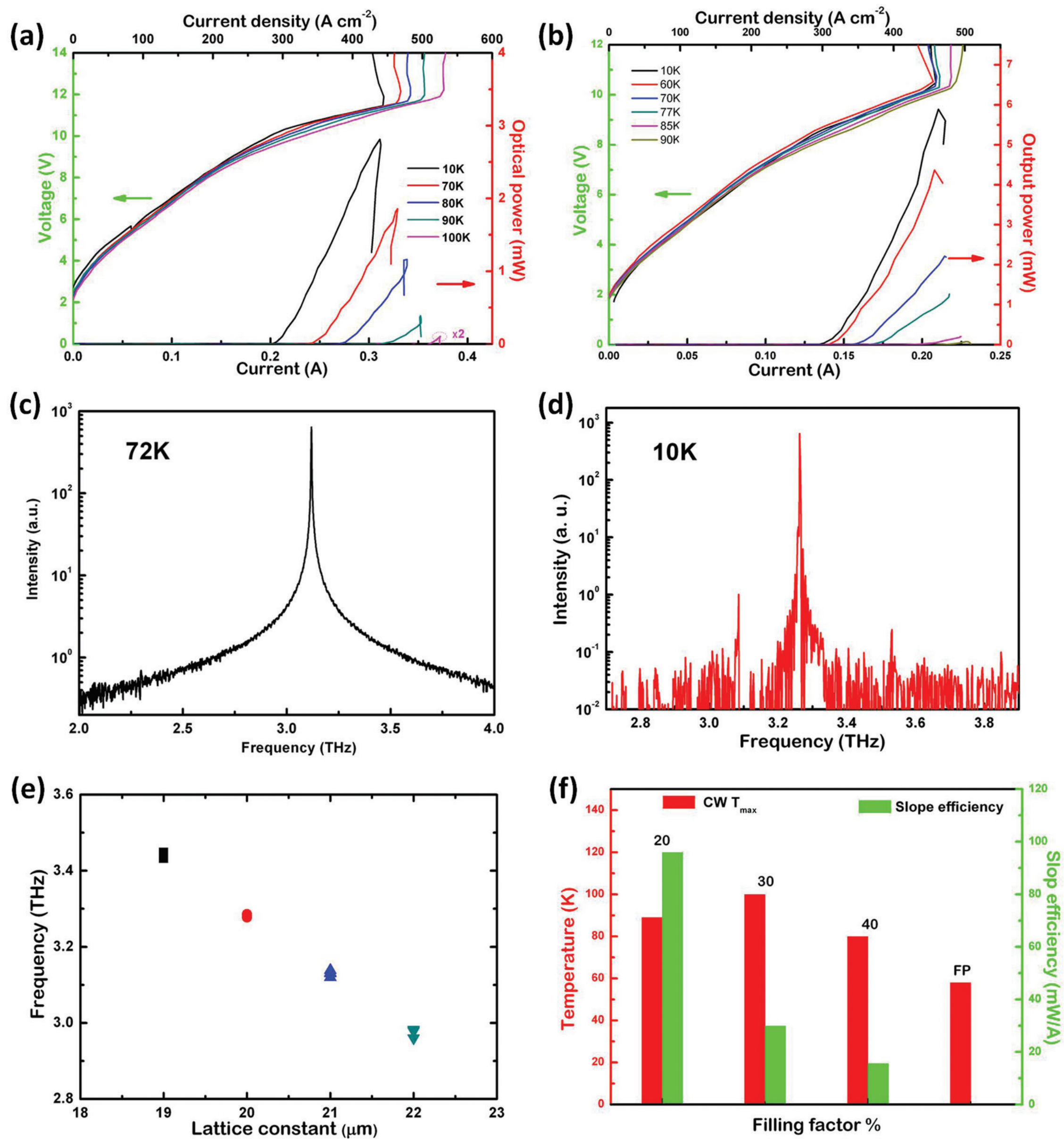

Figure 3 CW light-current-voltage (LIV) and T_{max} characterizations. (a) CW LIV characteristics of the device (the diameter of the central pumping pad is 600 μm, filling factor is 30%) for different heat sink temperatures (10K to 100K). (b) CW LIV characteristics of the device (the diameter of the central pumping pad is 600 μm, filling factor is 20%) for different heat sink temperatures (10K to 90K). (c) The lasing spectrum of the device shown in 3a measured at heat sink temperature 72 K. (d) The lasing spectrum of the device shown in 3b measured at heat sink temperature 10 K. (e) The photolithography tuning of devices (filling factor 30%) with different lattice constants (19, 20, 21 and 22 μm). (f) Experimental maximum CW operation temperature (in red bar) and slope efficiency (in green bar) of different filling factor (20%, 30% and 40% with the same size, the diameter of the central pumping pad is 600 μm) and FP laser (1000 $\times$ 150 μm^2 on the same QC layer).

to 89 K of 20% device. This indicates the existence of the optimal filling factor for CW operation, which in this case is around 30%.

A well-controlled far-field beam pattern is another critical feature of an efficient laser device. Fig. 4b and 4c (the same device measured in Fig. 3a) show the measured vertically emitted far field patterns of two devices (the diameter of the central pumping pad is 600 μm, filling factor is 30%) without and with the optimized Bragg extractor respectively. The device without Bragg extractor has a highly divergent beam pattern as shown in previous simulations (Fig. 2). The far field patterns of the device with the optimized Bragg extractor show a highly collimated beam pattern with a central lobe range of 10 degrees in both directions. The phase relation between the emission from the opposite Bragg extractors can be controlled by design, which should lead to a dough nut shape or a real single lobe far field respectively [21, 27].

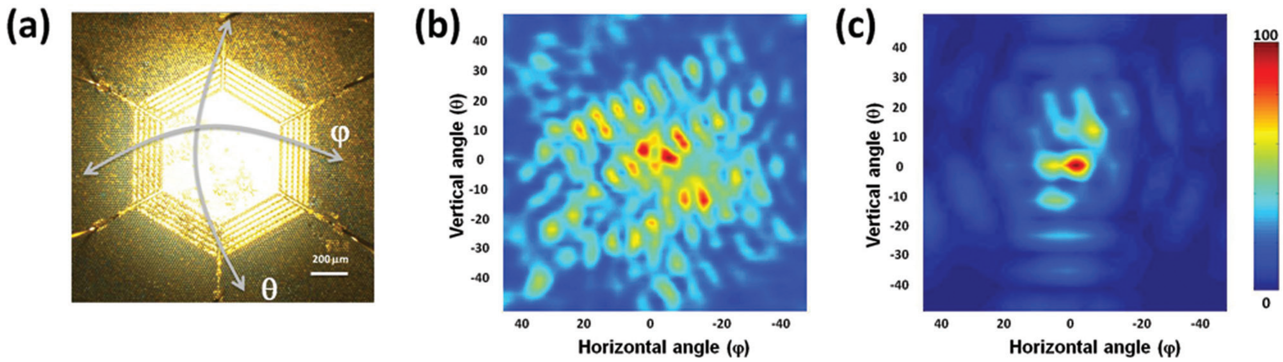

Figure 4 Far field characterizations. (a) Device is scanned both in vertical (θ) and horizontal (φ) directions for far field measurements. (b) Far field pattern of a device (600 μm diameter, filling factor is 30%, a is 21 μm) without Bragg extractor. (c) Far field pattern of a device (600 μm diameter, filling factor is 30%, a is 21 μm) with Bragg extractor.

4. Conclusions

In this letter, we have demonstrated that by utilizing a Bragg extractor to realize vertical emission and by introducing a PhC structure to achieve large pumping efficiency with better heat flow dissipation. This work brings the CW operation of THz semiconductor lasers to a new level. Single mode surface emission with several milliwatts output power is observed at 3.12 THz. Thanks to the scalability of PhCs, this design can be applied throughout the entire THz wavelength range, especially for longer wavelengths. Further fine optimization can still be performed depending on the final applications or the required figures of merit. Larger devices can contribute for higher output power. A further optimized extractor design can help for a collimated far field pattern and larger extraction efficiency. A variety of real applications of the CW operation THz light sources can be achieved in the future with optimized slope efficiencies and remarkable output powers above the liquid nitrogen temperature.

Acknowledgements. This work was supported by the Swiss National Centre of Competence in Research Quantum Photonics.

Received: 6 March 2013, **Revised:** 30 May 2013,
Accepted: 28 June 2013

Published online: 23 July 2013

Key words: Terahertz, quantum cascade laser, photonic crystal, surface emission, continuous-wave operation.

References

[1] J. Faist, F. Capasso, D. L. Sivco, C. Sirtori, A. L. Hutchinson, and A. Y. Cho, Science **264**, 553–556 (1994).
[2] R. Kohler, A. Tredicucci, F. Beltram, H. E. Beere, E. H. Linfield, A. G. Davies, D. A. Ritchie, R. C. Iotti, and F. Rossi, Nature **417**, 156–159 (2002).
[3] B. S. Williams, Nat Photonics **1**, 517–525 (2007).
[4] G. Scalari, C. Walther, M. Fischer, R. Terazzi, H. Beere, D. Ritchie, and J. Faist, Laser Photonics Rev **3**, 45–66 (2009).
[5] E. Strupiechonski, D. Grassani, D. Fowler, F. H. Julien, S. P. Khanna, L. Li, E. H. Linfield, A. G. Davies, A. B. Krysa, and R. Colombelli, Appl. Phys. Lett. **98** (2011).
[6] L. Mahler, A. Tredicucci, F. Beltram, C. Walther, J. Faist, B. Witzigmann, H. E. Beere, and D. A. Ritchie, Nat Photonics **3**, 46–49 (2009).
[7] R. Colombelli, K. Srinivasan, M. Troccoli, O. Painter, C. F. Gmachl, D. M. Tennant, A. M. Sergent, D. L. Sivco, A. Y. Cho, and F. Capasso, Science **302**, 1374–1377 (2003).
[8] Y. Chassagneux, R. Colombelli, W. Maineult, S. Barbieri, H. E. Beere, D. A. Ritchie, S. P. Khanna, E. H. Linfield, and A. G. Davies, Nature **457**, 174–178 (2009).
[9] M. I. Amanti, M. Fischer, G. Scalari, M. Beck, and J. Faist, Nat Photonics **3**, 586–590 (2009).
[10] G. Y. Xu, R. Colombelli, S. P. Khanna, A. Belarouci, X. Letartre, L. H. Li, E. H. Linfield, A. G. Davies, H. E. Beere, and D. A. Ritchie, Nature Communications 3 (2012).
[11] H. Zhang, L. A. Dunbar, G. Scalari, R. Houdre, and J. Faist, Optics Express **15**, 16818–16827 (2007).
[12] H. Zhang, G. Scalari, M. Beck, J. Faist, and R. Houdre, Optics Express **19**, 10707–10713 (2011).
[13] P. H. Siegel, Ieee T Microw Theory **50**, 910–928 (2002).
[14] M. Tonouchi, Nat Photonics **1**, 97–105 (2007).
[15] B. Ferguson and X. C. Zhang, Nat Mater **1**, 26–33 (2002).
[16] D. Mittleman, Sensing with terahertz radiation, Springer, Berlin, New York, (2003).
[17] B. S. Williams, S. Kumar, Q. Hu, and J. L. Reno, Optics Express **13**, 3331–3339 (2005).
[18] L. Mahler, A. Tredicucci, R. Kohler, F. Beltram, H. E. Beere, E. H. Linfield, and D. A. Ritchie, Appl. Phys. Lett. 87 (2005).
[19] M. S. Vitiello, G. Scamarcio, V. Spagnolo, S. S. Dhillon, and C. Sirtori, Appl. Phys. Lett. 90 (2007).
[20] G. Sevin, D. Fowler, G. Xu, F. H. Julien, R. Colombelli, H. Beere, and D. Ritchie, Electron Lett **46**, 1513–U1559 (2010).
[21] Y. Chassagneux, R. Colombelli, W. Maineult, S. Barbieri, S. P. Khanna, E. H. Linfield, and A. G. Davies, Appl. Phys. Lett. 96 (2010).

[22] H. Zhang, G. Scalari, J. Faist, L. A. Dunbar, and R. Houdre, J Appl Phys 108 (2010).
[23] S. Kumar, B. S. Williams, Q. Qin, A. W. M. Lee, Q. Hu, and J. L. Reno, Optics Express **15**, 113–128 (2007).
[24] M. I. Amanti, G. Scalari, R. Terazzi, M. Fischer, M. Beck, J. Faist, A. Rudra, P. Gallo, and E. Kapon, New J Phys 11 (2009).
[25] J. A. Fan, M. A. Belkin, F. Capasso, S. Khanna, M. Lachab, A. G. Davies, and E. H. Linfield, Optics Express **14**, 11672–11680 (2006).
[26] M. I. Amanti, G. Scalari, M. Beck, and J. Faist, Optics Express **20**, 2772–2778 (2012).
[27] C. J. S. de Matos and J. R. Taylor, Appl. Phys. Lett. **83**, 5356–5358 (2003).